PFC/RR-89-18

SAFETY AND PROTECTION FOR LARGE-SCALE MAGNET SYSTEMS – FY89 REPORT

R.J. Thome, M. Oshima, R.D. Pillsbury, Jr., W.R. Mann

March 1990

Plasma Fusion Center
Massachusetts Institute of Technology
Cambridge, Massachusetts 02139

Submitted to
Idaho National Engineering Laboratory
Idaho Falls, Idaho

Table of Contents

Section	Title	Page No.
I	Introduction	1
II	Computation of Quench Propagation in Multiple Superconducting Coils	2
2.1	Introduction	
2.2	Description of Quench Analysis Program	3
2.3	Analysis Results	12
2.3.1	Analyses for a Single-Coil System	12
2.3.2	Analysis of Four-Coil System	23
2.4	Conclusion	27
III	Torsional Shear Development in Central Solenoids	31
3.1	Introduction	31
3.2	Torsional Shear Stress	32
	Bibliography	34

I. Introduction

The large magnet safety and protection effort this fiscal year focused on two areas: (1) the continued development of a transportable, safety-oriented code for study of quench characteristics in large magnets and (2) the initial modeling of shear stress effects in the central solenoid of a tokamak resulting from the twisting of the toroidal field coils in a "bucked" type of design.

The first phase of our quench program development activity is complete. It was the subject of an Engineers/Masters thesis (M. Oshima) in the Nuclear Engineering Department. The result is a code for coils with epoxy impregnated windings that employs a unique one-dimensional, logical coordinate system to solve the three-dimensional problem. We believe that, with further development, this approach will be particularly efficient numerically and applicable to coils wound with cable-in-conduit conductors and to bath-cooled cases. The code can treat quench transients in a general configuration of multiple, inductively coupled coils, three-dimensional normal front propagation, and material properties which are dependent on the local magnetic fields which are functions of space and of time. Thus far the code has only been applied to simple solenoidal cases, but has shown good agreement with measured data in the form of a characteristic quench time. Modifications to improve efficiency and modeling accuracy are under way together with comparisons with other test data.

We have also begun a modeling activity to gain insight into the interaction between the TF coils and the central solenoid in a generic "bucked" tokamak configuration in which the TF coil centering forces and twist due to the overturning moments are partially transmitted to the central solenoid. The coupling at the interface between the two subsystems can be the cause of excessive shear stresses in the solenoid and subsequent failures (e.g., shear keys in the central solenoid in JET). Thus far we have a somewhat oversimplified model which clearly shows the interactions and importance of the friction coefficient at the outer diameter of the central solenoid in this type of system. We will continue development of this model next year to incorporate more realistic boundary conditions and apply it to selected cases in actual machines which have been built (e.g., JET) or which are being considered for construction (e.g., CIT).

II. Computation Of Quench Propagation in Multiple Superconducting Coils

2.1 Introduction

This section will summarize the capabilities and preliminary results from a computer program [1] written to to analyze quench propagation in multiple superconducting coils.

A "quench" is the nonrecoverable transition of a superconducting wire section to the normal state and the normal region grows with time. In this event, a large amount of energy can be released in a relatively short time. This can result in overheating and/or voltage breakdown of superconducting coils during a quench. In order to protect against overheating and voltage breakdown, it is important to predict the coil characteristic behavior such as temperature and voltage distributions during a quench.

The program has the following four features:

1. application to a general configuration of multiple coils
2. application to multiple, inductively coupled coils
3. three dimensional normal front propagation
   - longitudinal direction (along wire)
   - transverse direction
     (from turn to turn and from layer to layer)
4. material properties dependent on magnetic field, which is varying in time and space

The three-dimensional quench propagation problem was solved as a one-dimensional problem by using a logical coordinate system. The details are discussed in the following section.

The code was applied to a single coil system. The single coil system is composed of an epoxy-bonded NbTi wire, and some of the quench data for this system were available. As a result of the calculation, the importance of three-dimensional analysis was demonstrated.

The comparisons with experimental data showed that the computed quench time ($\tau_o = \frac{I_o}{(dI/dt)_{max}}$) at the high initial currents correlated with the experimental data very well, while it began to deviate at the low intial currents. The divergence at the lower initial currents was caused by two effects: 1.) limited critical current characteristic data, and 2.) lack of consideration of heat conduction between normal elements in the computation.

A four-coil system was analyzed to demonstrate code capability and the importance of inductive coupling among coils during a quench. The hypothetical four-coil system was modeled: one superconducting coil and three normal coils which could have three different types of normal resistivity (1.) 316 stainless steel, 2.) copper, and 3.) quasi–superconductor whose magnitude of resistivity is 10^{-3} times copper). The computed results indicated that the temperature rise in the quenching coil can be reduced by combining superconducting coils with the lower resistivity inductively coupled coils.

2.2 Description of Quench Analysis Program

The computer program "PQUENCH" was designed to simulate three-dimensional quench propagation and its consequences. The program has the following features:

- application to a general configuration of multiple coils such as solenoids or toroidal coils by using a logical coordinate system,
- calculation of the circuit current transients in multiple, inductively coupled coils,
- normal front propagation in the longitudinal (along the wire) and the transverse directions (from turn to turn and from layer to layer through the windings), and
- material properties dependent on magnetic field magnitude (varying in space and time)for the matrix (copper and aluminum) and superconducting materials (NbTi).

Fig. 2.1 describes the relationship between real space and a logical coordinate system for an example of a 4 layer $\times$ 5 turn solenoid with ten elements

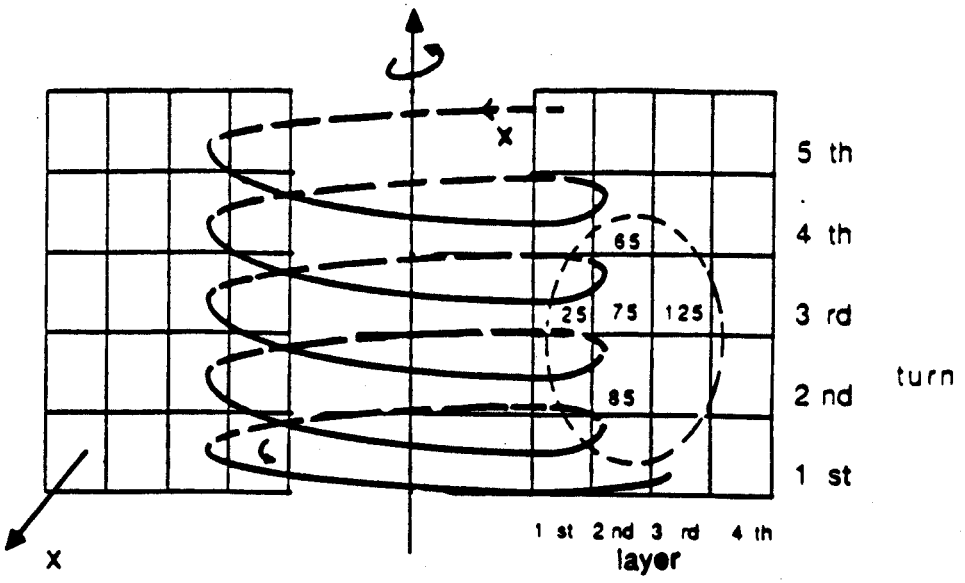

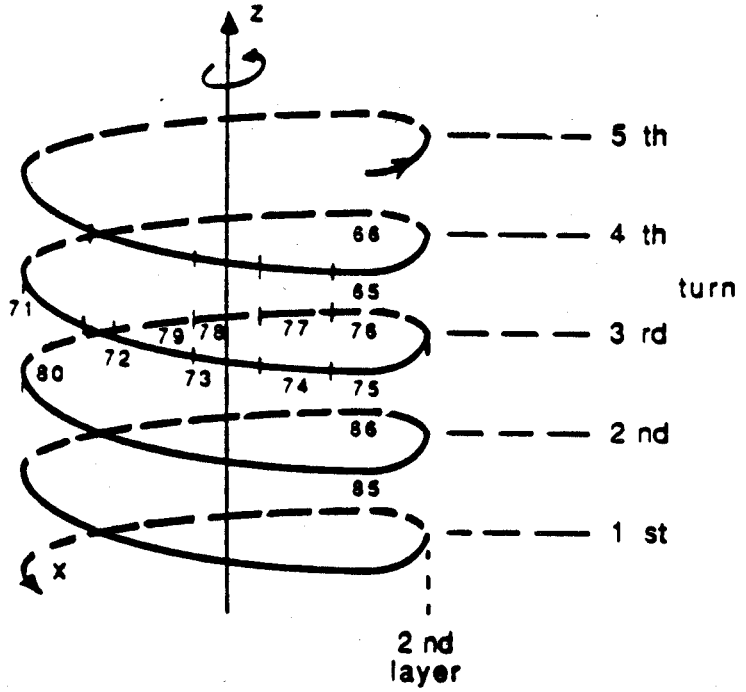

Figure 2.1: Schematic illustration of relationship between real space and a logical coordinate system for a 4 layer X 5 turn solenoid coil

in each turn. The computer program assumes that the magnet system consists of a number of long wires connected end to end, and each wire is divided into finite length elements. Each element is numbered and correlated with geometry-related information such as length, local magnetic field influence coefficients, and relationship to adjacent elements. The advantage of this logical coordinate system is that a three–dimensional problem in real space can be transformed to a one–dimensional problem by keeping track of the initiation of new quench regions and the normal front elements in each quench region.

Figs. 2.2 and 2.3 give the flow-chart for the program. After the program obtains the conductor and system geometry information based on a logical coordinate system, the normal front propagation in the longitudinal and transverse directions is calculated. Fig. 2.4 shows a logical coordinate system in the vicinity of the element 75 as an example. The longitudinal normal front propagates along a wire in the backward moving direction to the element 74 (U_{lb} in Fig. 2.4) and in the forward direction to the element 76 (U_{lb} in Fig. 2.4). The transverse propagation conducts in the direction from the element 75 to the elements 65 (U_{tt_+} in Fig. 2.4) and 85 (U_{tt_-} in Fig. 2.4) as a turn–to–turn propagation, and from the element 75 to the elements 25 (U_{tl_-} in Fig. 2.4) and 125 (U_{tl_+} in Fig. 2.4) as a layer–to–layer propagation.

For the propagation along a wire, the normal front is assumed to move with a velocity given by [2]:

$$U_l = \frac{j_{mat}}{(\gamma C_p)_{av}} \{ \frac{\rho k_{av}}{T_t - T_b} \}^{\frac{1}{2}} \tag{2.1}$$

where

$$(\gamma C_p)_{av} = \frac{1}{1 + \lambda + \frac{\lambda}{\lambda'} F_{vel}} \left[(\gamma C_p)_{sc} + \lambda (\gamma C_p)_{mat} + \frac{\lambda}{\lambda'} F_{vel} (\gamma C_p)_{in} \right] \tag{2.2}$$

$$k_{av} = \frac{\lambda}{1 + \lambda + \frac{\lambda}{\lambda'} F_{vel}} k_{mat} \tag{2.3}$$

$$\tag{2.4}$$

U_l is the longitudinal velocity, j_{mat} is the current density in the matrix material, and ρ is the electrical resistivity. The variable (γC_p) is the volumetric specific heat, k is the thermal conductivity. The subscripts av, sc, mat

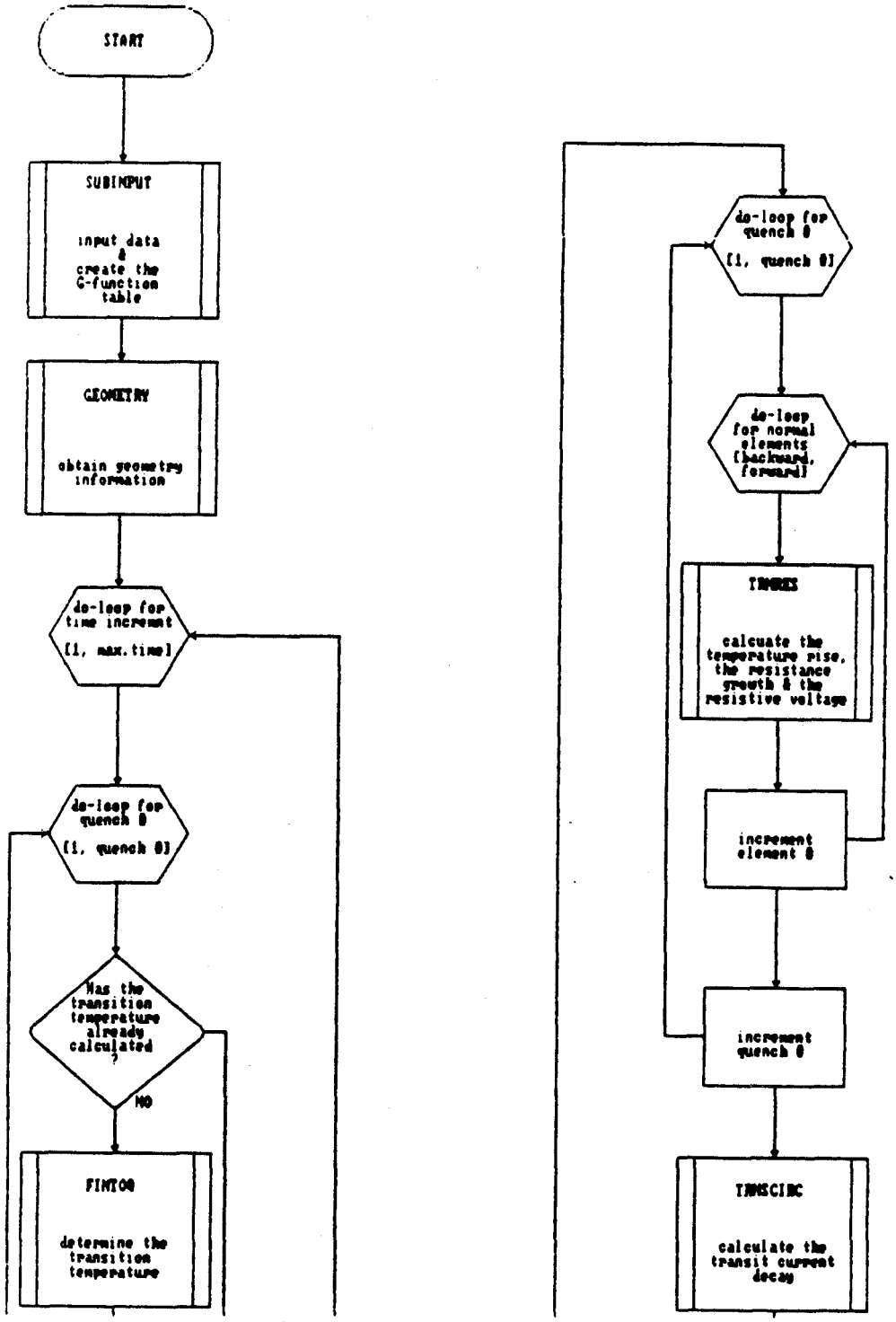

Figure 2.2: Flow Chart of program PQUENCH – part 1 – (Note: Flow chart continues on the next page.)

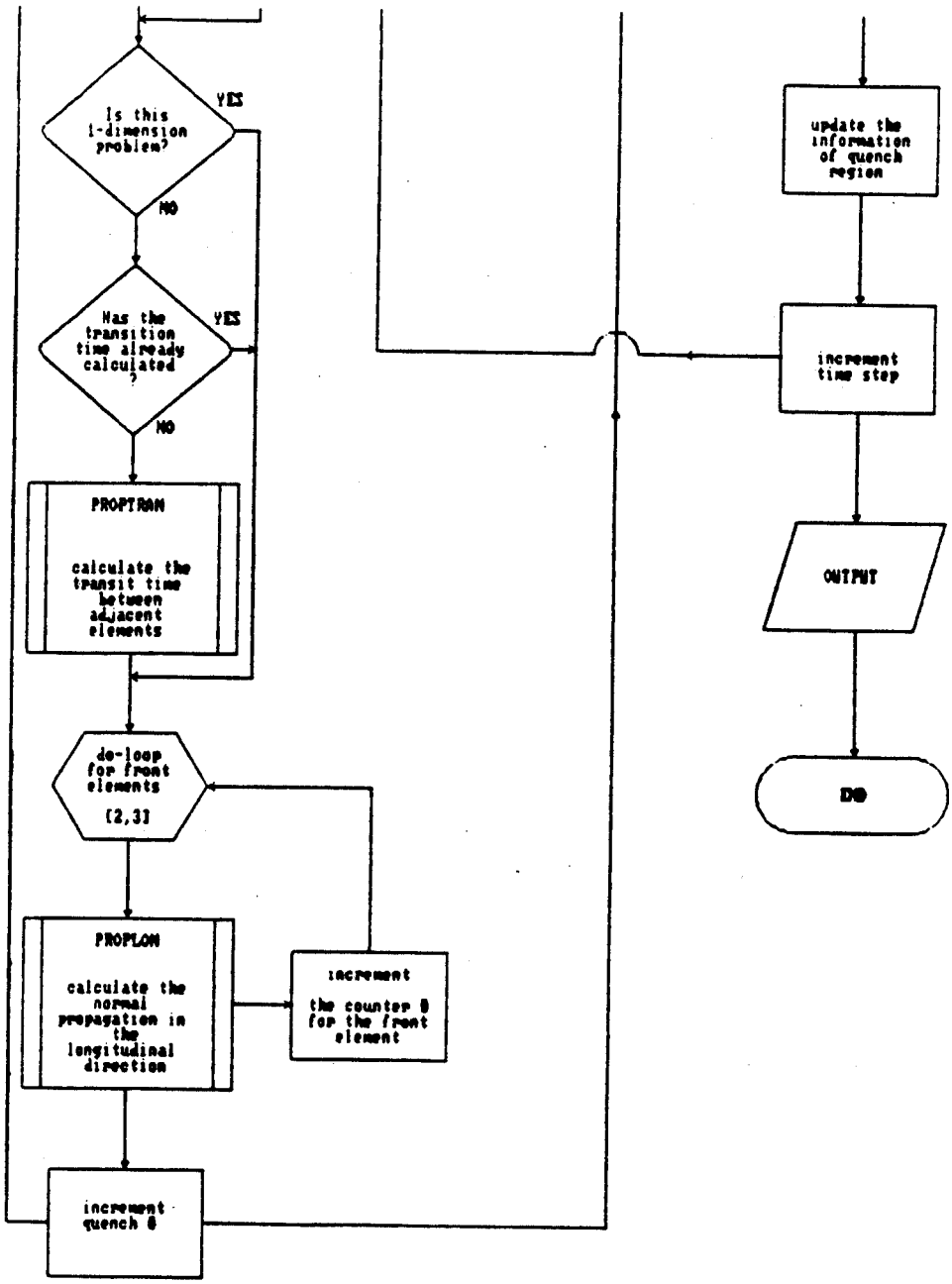

Figure 2.3: Flow Chart of program PQUENCH – part 2 – (Note: This part of flow chart is continued from the previous page.)

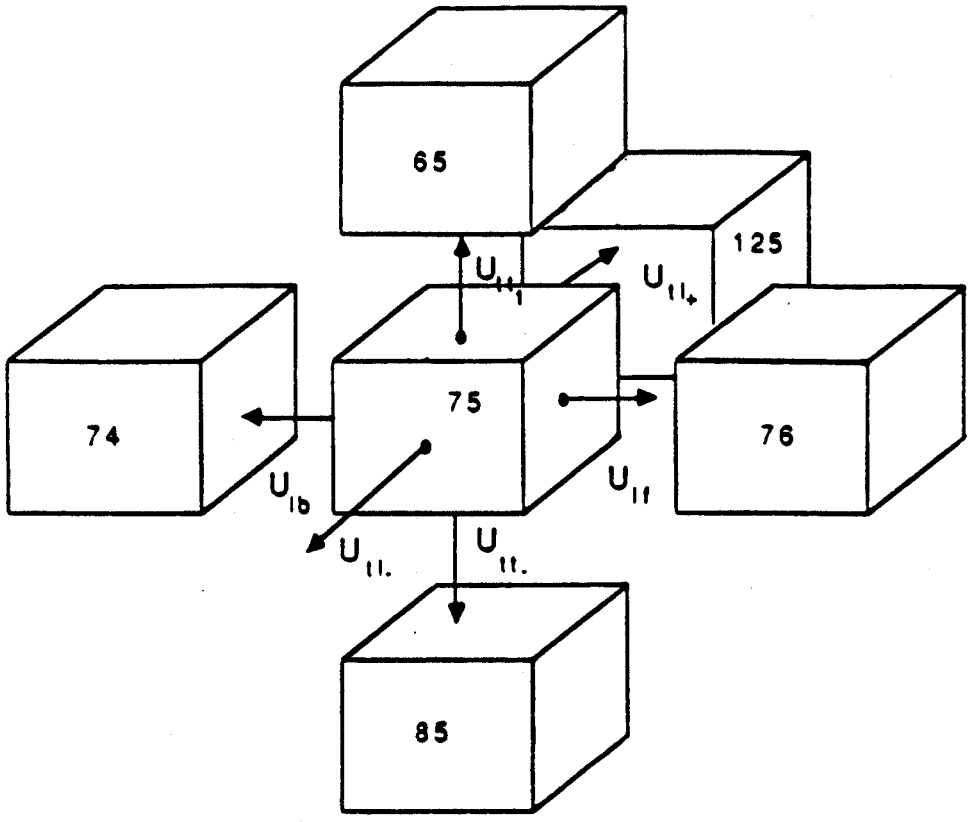

Figure 2.4: Schematic illustration of the adjacent element and the normal front propagation for the element 75

and *in* represent averaged properties over the composite conductor cross–section, superconducting material, matrix material, and insulator material, respectively. The variable λ is the volume ratio of matrix to superconducting material, and λ' is the volume ratio of matrix to insulator material. Temperature T_b is the bath temperature and T_t is the transition temperature defined as [3]:

$$T_t = T_{cs} + \frac{2}{3}(T_c - T_{cs}) \tag{2.5}$$

where T_c is the critical temperature, and T_{cs} is the current sharing temperature. The factor F_{vel} is the fraction of heat which diffuses into the insulator material and is defined as:

$$F_{vel} = \frac{\Delta t}{(\tau_t)/2)} \tag{2.6}$$

where Δt is the size of the computational time increment, and τ_t is the transit time.

After the longitudinal velocity was determined based on Eq. 2.1, the length over which the normal region propagated in the time Δt, $l_{parallel}$, is calculated:

$$l_{parallel} = U_l \Delta t. \tag{2.7}$$

Since $l_{parallel}$ is the length in real space, this length was converted to the number of logical elements corresponding to the computed length and its location. The information about the normal front elements along a wire is stored in an array and is updated in each time step.

For the transverse propagation, the transit time τ_t is defined as the characteristic time for the heat at a quenched element to raise the temperature of the adjacent element to the critical temperature. The transit time is used as the indicator for onset of a new quench region at the transverse adjacent element. The transit time τ_t is obtained for turn–to–turn and layer–to–layer propagation by solving the following equation with the Newton-Raphson method [3]:

$$\frac{\tau_t^2}{2} - \frac{\tau_{in}}{4}\tau_t + \left(\frac{\tau_{in}}{4}\right)^2 \left[1 - exp\left(\frac{-4\tau_t}{\tau_{in}}\right)\right] = \frac{R_{in}}{\theta}\left[A_{sc}\int_{T_b}^{T_{tt}} (\gamma C_p)_{sc} dT + A_{mat}\int_{T_b}^{T_{tt}} (\gamma C_p)_{mat} dT\right] \tag{2.8}$$

where, τ_{in} is the characteristic time constant expressed as $\tau_{in} = R_{in}c_{in}$. The definition of R_{in}, c_{in} and θ is:

$$c_{in} = V_{in}\frac{\int_{T_b}^{T_{ts}}(\gamma C_p)_{in}dT}{(T_{ts}-T_b)} \tag{2.9}$$

$$R_{in} = \frac{1}{k_{in}}\frac{\Delta r_{in}}{A_{in}} \tag{2.10}$$

$$\theta = \frac{\rho j_{mat}^2}{(\gamma C_p)_{av}}. \tag{2.11}$$

A_{in}, V_{in}, and Δr_{in} are the area, volume, and thickness of the insulator between conductors. T_{ts}, and T_{tt} are the transition temperature of the source element, and transition temperature of the target element.

After information about the extent of the normal front propagation is obtained during a time step, the temperature rise at each normal element and the growth of the conductor resistance are calculated. Fig. 2.5 shows a schematic illustration of the temperature rise in a 4 layer $\times$ 5 turn solenoid after 5 time increments. Assume that the first quench started at the element 25. The normal front propagates discretely in terms of the number of elements as shown in Fig. 2.5. The figure also shows the quench initiation at the elements 15, 35, and 75 by the transverse heat conduction from the element 25. Since the magnetic dependence of properties were considered, the propagation speed could be different in different directions (note the difference in the manner of the temperature rise between the elements 15 and 35).

The incremental current decay associated with the normal region growth is then determined by solving the following coupled lumped parameter circuit equation [4,5]:

$$[L]\left\{\frac{dI}{dt}\right\} + [R_d + R_R(t)]\{I\} = \{V(t)\} \tag{2.12}$$

where $[L]$ is the inductance matrix, $[R_d]$ is the dump resistor matrix, and $\{I\}$ and $\{V\}$ are current and voltage vectors. The variable $[R_R(t)]$ is the resistance resulting from the growth of the normal resistive zone, and is varied with each time step.

Quench information is updated at each time step, and the onset of new quench regions based on the transit time is evaluated after the current decay calculation. If the total elapsed time is longer than the transit time at

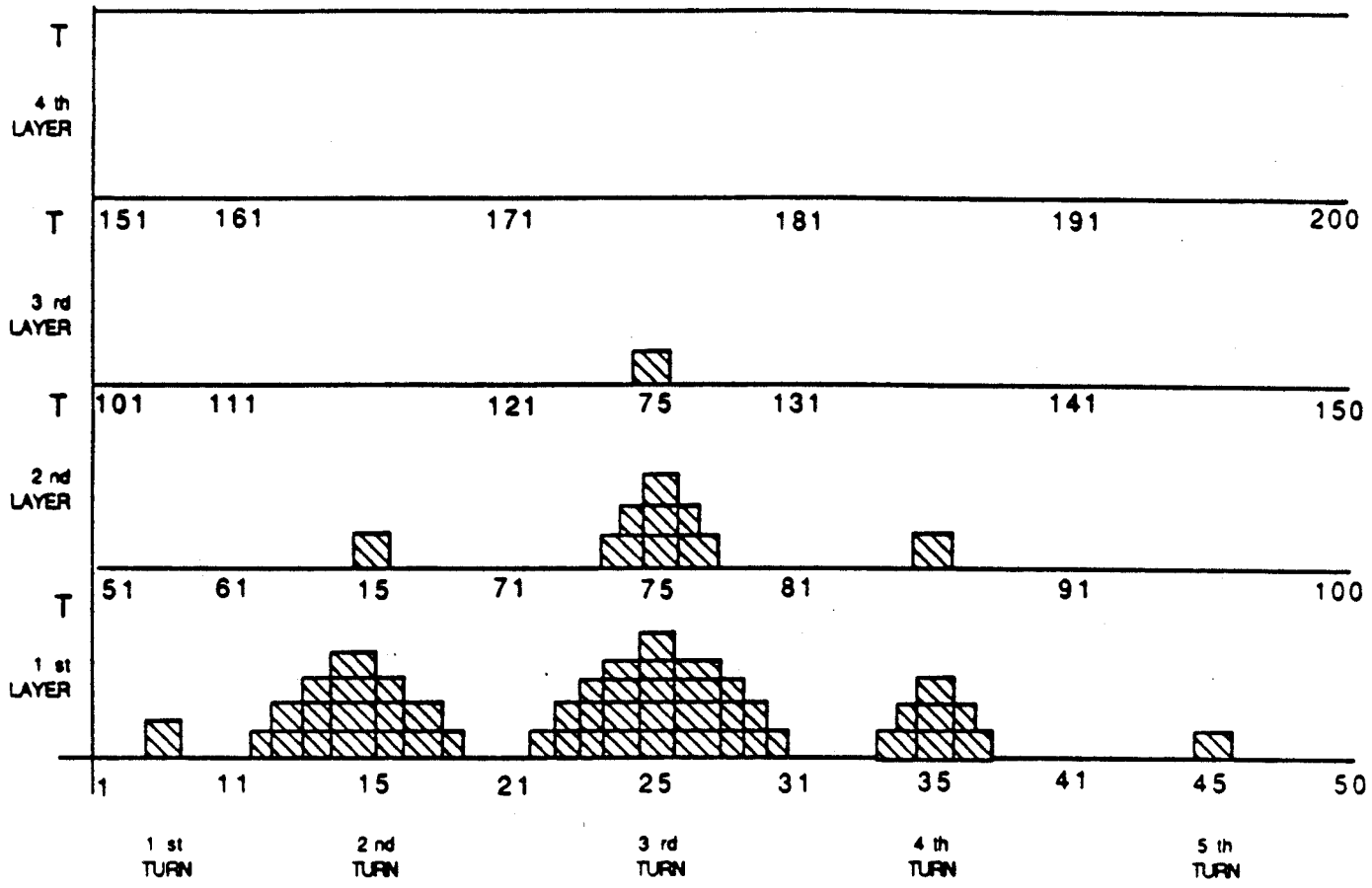

Figure 2.5: Schematic illustration of the temperature rise in a 4 layer X 5 turn solenoid coil

a quench region, it indicates that a new quench region has started at an adjacent element.

The time step is updated and the computer procedure continues until the total time achieves the maximum allowed by input data.

2.3 Analysis Results

2.3.1 Analyses for a Single-Coil System

The geometry of the single-coil system is shown in Fig. 2.6, and some of the features of the single coil are also given. The system is composed of an epoxy-bonded NbTi superconductor. Some quench data for this conductor and characteristic data (critical current vs. magnetic field) were available.

There were 16 layers and 78 turns per layer. Thus, there were a total of 1248 turns in the winding. Each turn was modeled by 20 elements which resulted in 24960 elements in the system.

The computer program can calculate three types of quench propagation:

1. one-dimensional (longitudinal propagation only along the wire)
2. two-dimensional (longitudinal along the wire and from layer to layer or from turn to turn)
3. three-dimensional (longitudinal along the wire, from layer to layer, and from turn to turn)

In this coil system, the transverse propagation is important due to the compact and epoxy-impregnated design as is shown in Fig. 2.7. The computed current in the three–dimensional propagation decayed much faster than either the one- or two-dimensional calculations.

Fig. 2.8 shows the computed current decay versus time for initial currents of 400, 600, 800 A. As the initial current becomes higher, the current decays faster because the heating rate (ρj^2) are generally higher and increase the propagation rate.

In comparing the computed results with the experimental data, the following definition for quench time is used:

$$\tau_o = \frac{I_o}{(dI/dt)_{max}} \tag{2.13}$$

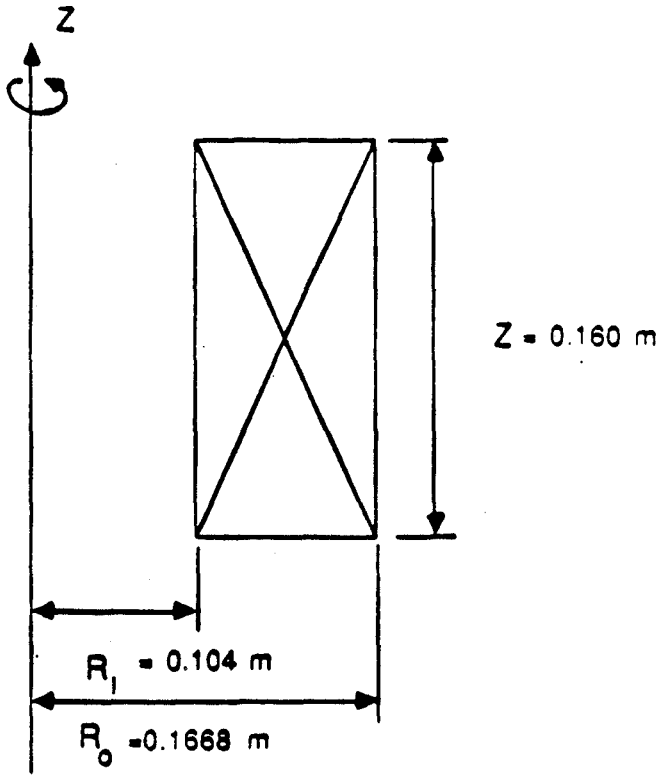

- System Characteristics -

Winding dimensions :		
inner radius, R_i	=	0.104 m
outer radius, R_o	=	0.168 m
length, Z	=	0.160 m
Winding information:		
No. of layers	=	16
No. of turns per layer	=	78
total no. of turns	=	1248

- Conductor Characteristics -

Superconducting material	:	NbTi
Matrix material	:	Copper
Insulator material	:	Epoxy
Conductor dimension, d_{con}	:	1.9 mm square
Insulator thickness, t_{in}	:	3.81×10^{-2} mm per side
Cu / S.C. ratio, λ	:	2.0

Figure 2.6: Geomtery of a single coil system

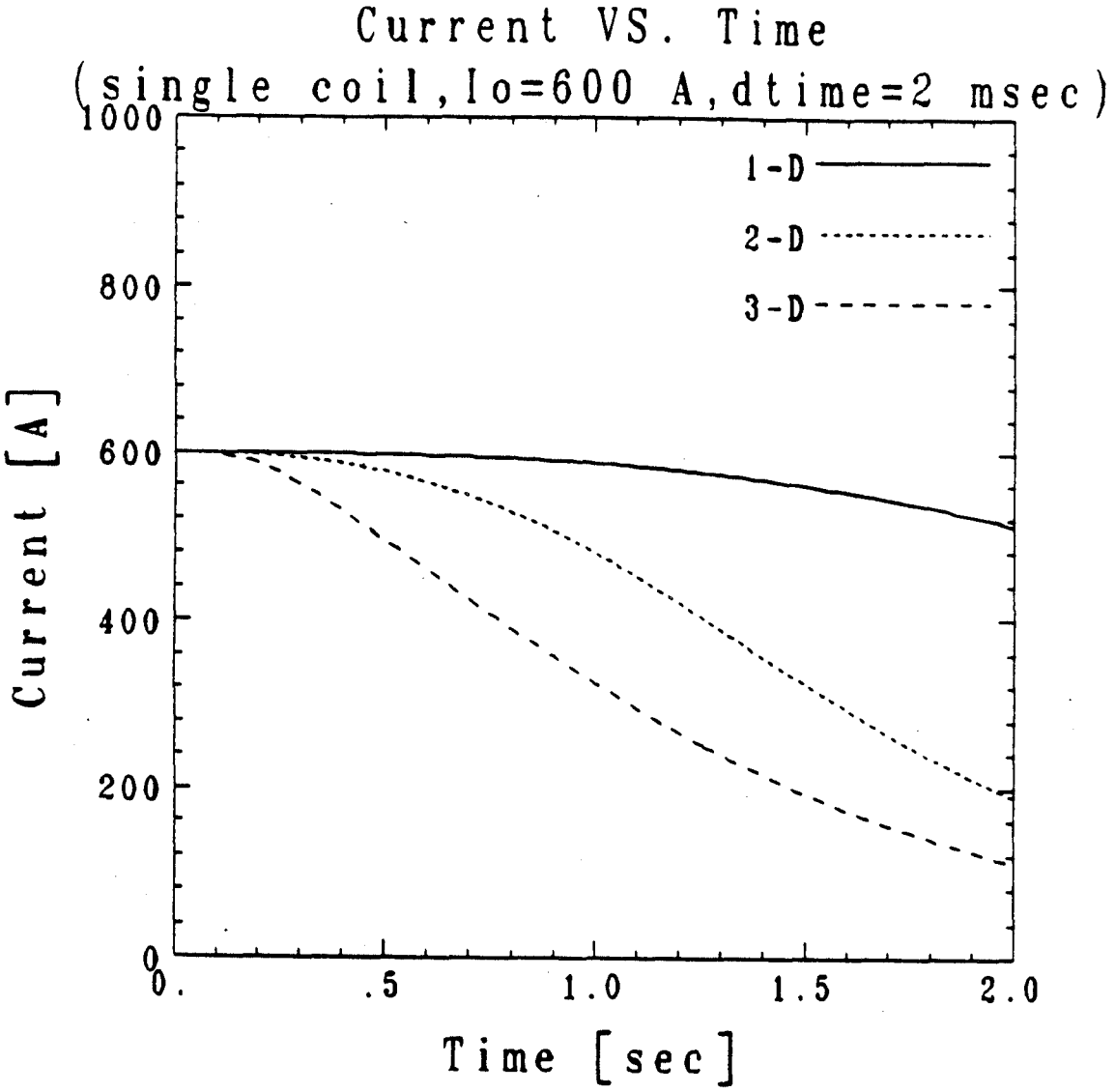

Figure 2.7: Calculated current decay versus time for an initial current of 600 A for 1–dimensional, 2–dimensional, and 3–dimensional quench propagation

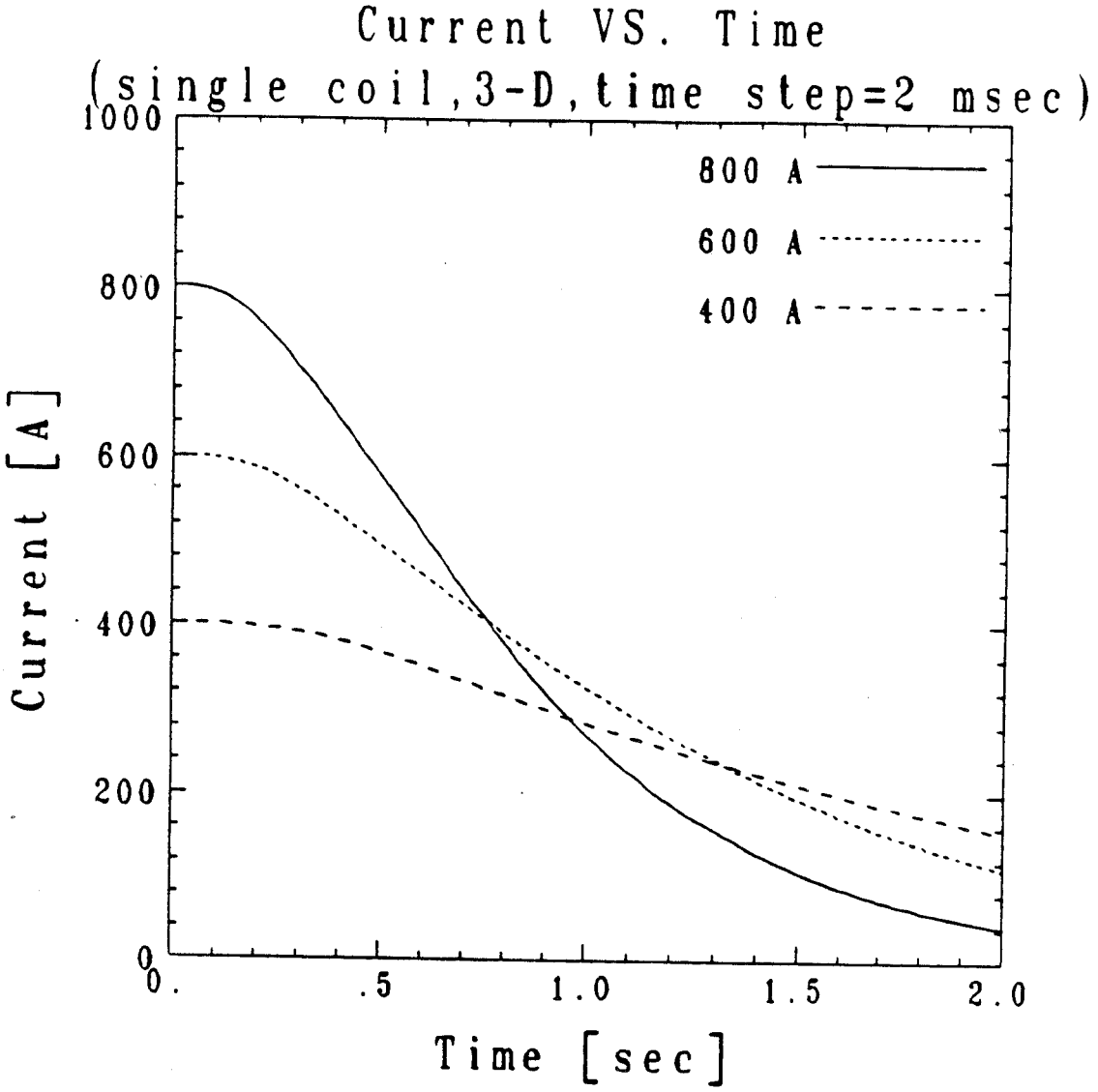

Figure 2.8: Calculated current decay versus time for an initial current of 400, 600, and 800 A

Fig. 2.9 summarizes the computed quench time τ_o and experimental quench time [6]. Note that calculations were only done for the epoxy bonded case. The result shows that the computed time correlates with the experimental result very well at high initial currents, but begins to deviate at the lower initial currents. This divergence at the low initial currents is explained by two effects. First, the correlation for the critical property values is uncertain at lower magnetic field because the data were not available. Experimental data for the dependence of the critical current on magnetic field is available only in the range between 5.0 and 8.0 T as shown in Fig. 2.10. At an initial current of 400 A, for example, the highest magnetic field (at the element in the inner layer on the mid–plane, which is the element 780) is 3.08 T. Hence, the critical values are calculated in the uncertain critical property range for the entire coil throughout the transient.

Secondly, the program considers heat conduction between normal and superconducting elements to initiate normal regions in adjacent elements which are originally in the superconducting state, but does not consider heat conduction between normal elements. Once an element becomes normal, it is treated adiabatically. The subsequent lack of heat conduction between normal elements is a good approximation for fast decay rates (cases with high initial currents). On the other hand, it will introduce errors in the calculation for slow decay rates (cases with low initial current) because the overall time scale for the process is long.

Figs. 2.11 and 2.12 shows the maximum temperature versus time for initial currents of 400, 600, and 800 A. Note that the higher energy dissipation rates associated with the higher initial current leads to higher maximum temperature and resistive voltage.

One of the important objectives for this thesis was to predict temperature and voltage distributions in superconducting coils. Fig. 2.13 shows the superimposed temperature distributions in the coil at time = 0.2, 0.5,1.0 and 2.0 sec for an initial current of 600 A for 3–dimensional propagation. Fig. 2.14 shows the temperature distributions during quench development at time = 0.002, 0.01, 0.02, 0.05, 0.1, 0.2, 0.5, 1.0, 1.5, and 2.0 sec.

Each sawtooth has a sharp peak corresponding to the element in the mid–plane, and there is a total of sixteen peaks. The sixteen sharp temperature peaks were developed due to the transverse quench propagation from layer to layer. The element with the highest temperature in the layer was the first to go normal in that layer. As shown in Fig. 2.14 at the early time, the

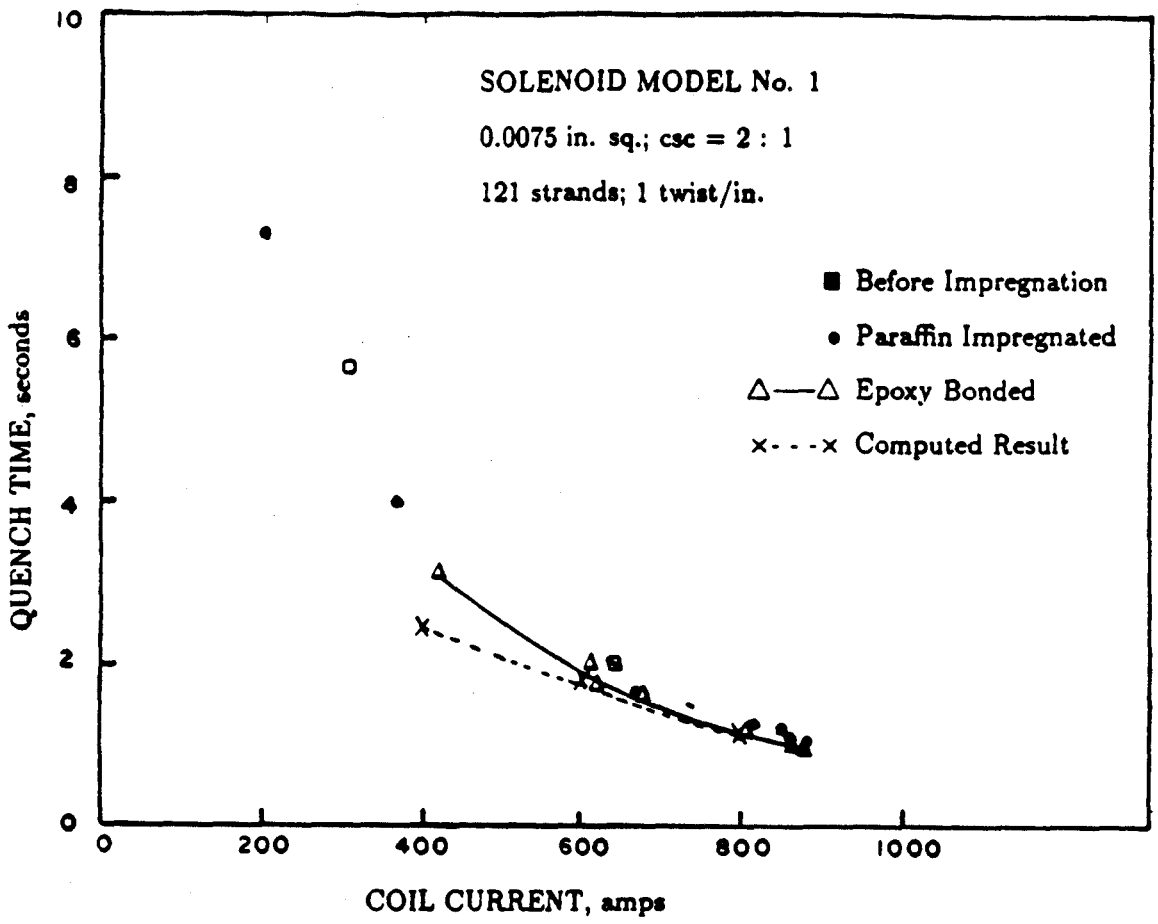

Initial current [A]	400	600	800
Computed Quench Time (τ_o) [sec]	2.34	1.71	1.17
Experimental Quench Time (τ_o) [sec]	3.36–3.28	1.84–1.92	1.18-1.25

Figure 2.9: Comparison of the computed quench time with experimental quench time

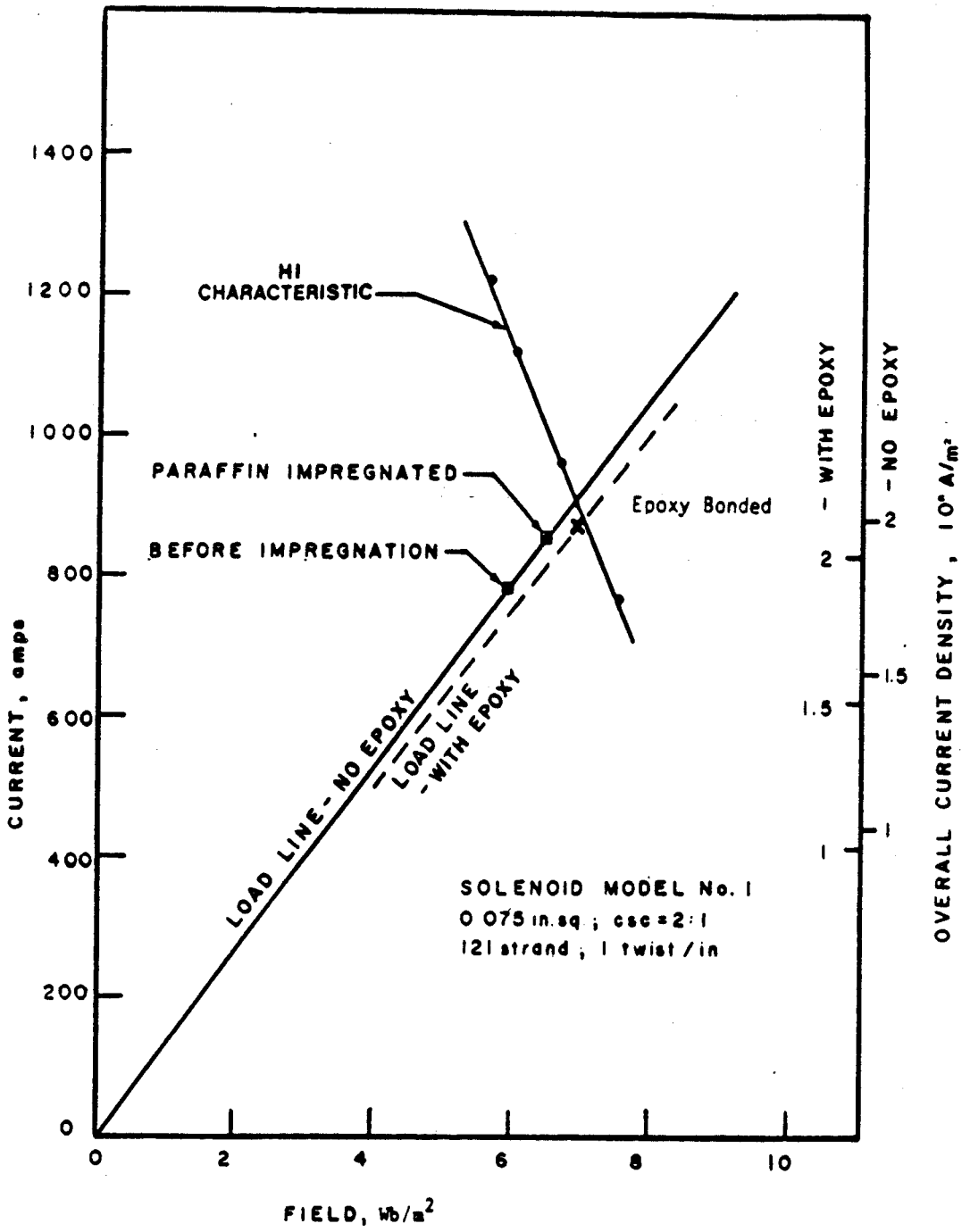

Figure 2.10: Characteristic relation between current and magnetic field for the conductor together with the load line for the solenoid [6]

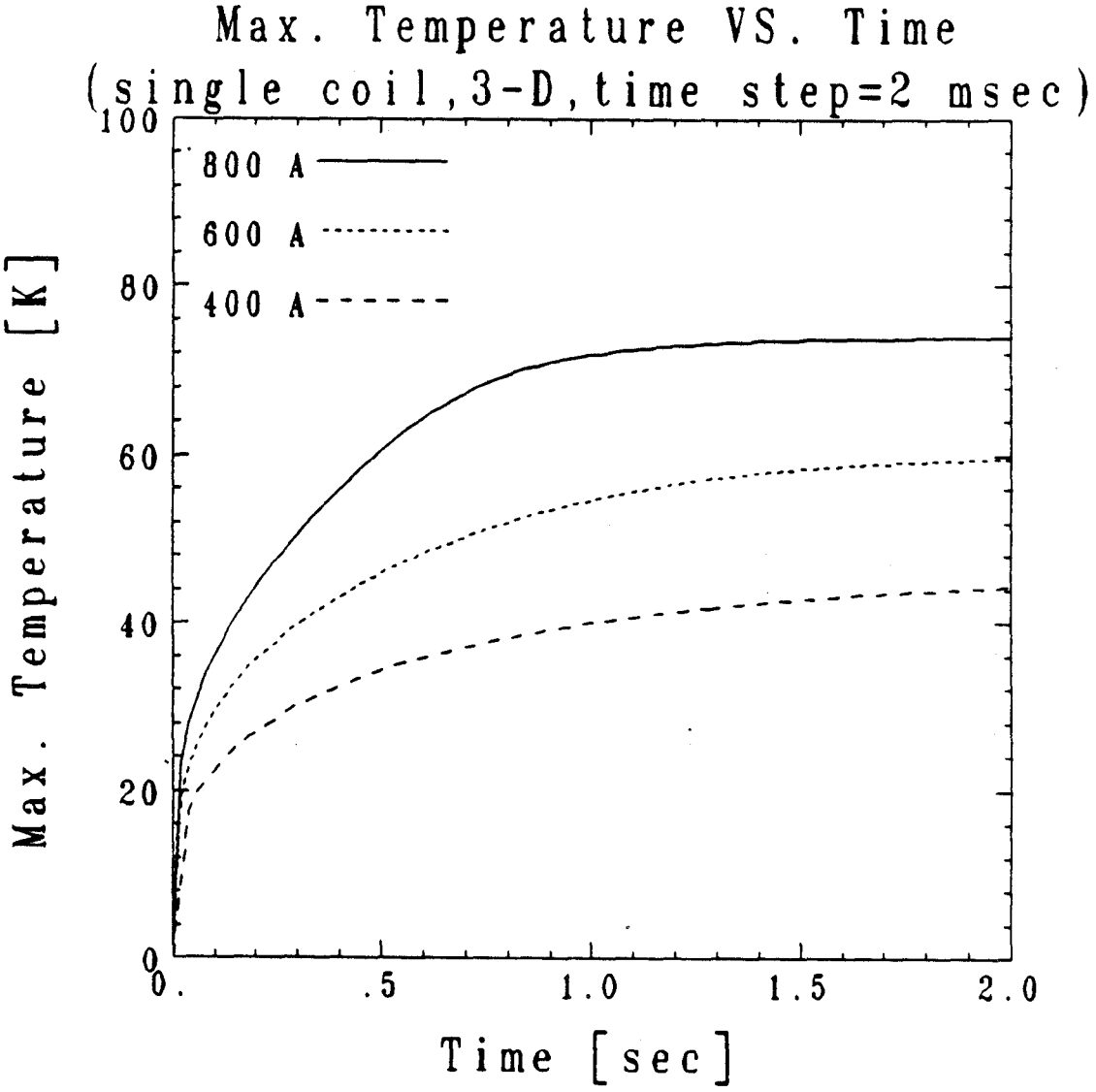

Figure 2.11: Calculated maximum temperature in coil versus time for initial currents of 400, 600, and 800 A

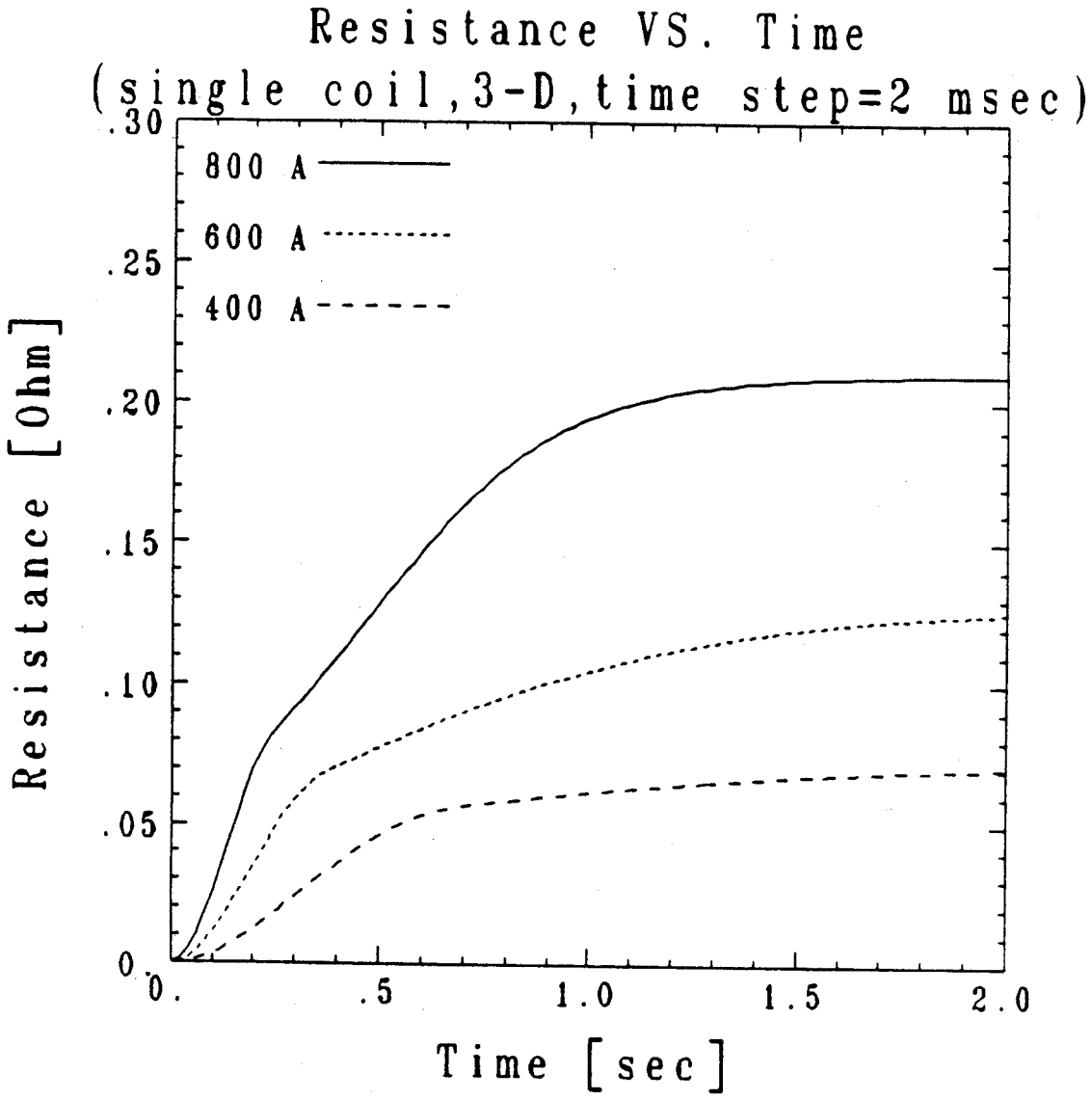

Figure 2.12: Calculated resistive voltage in coil versus time for initial currents of 400, 600, and 800 A

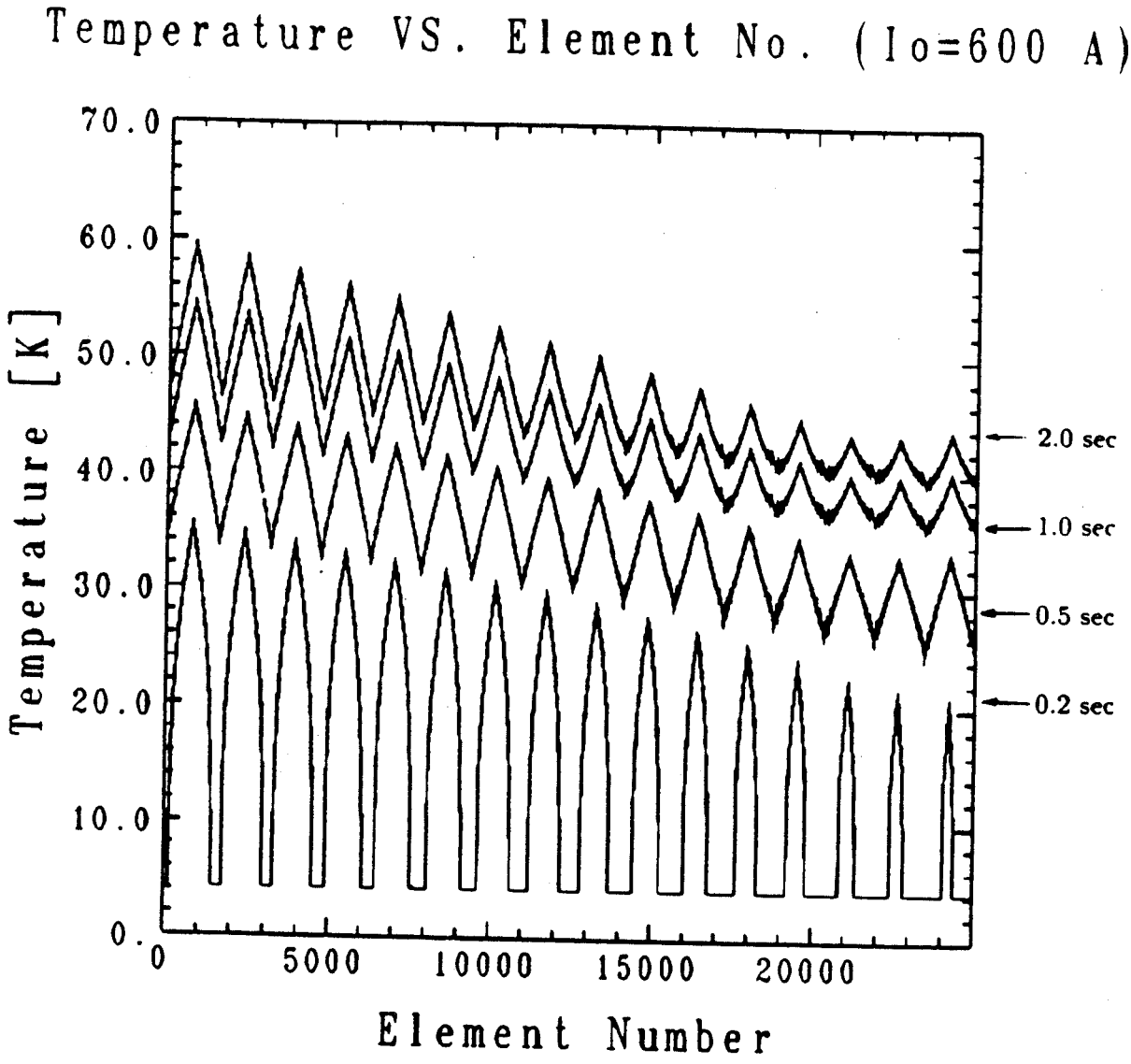

Figure 2.13: Temperature distribution in the coil versus at element number (1–24960) at selected times for an initial current of 600 A for a 3–dimensional propagation

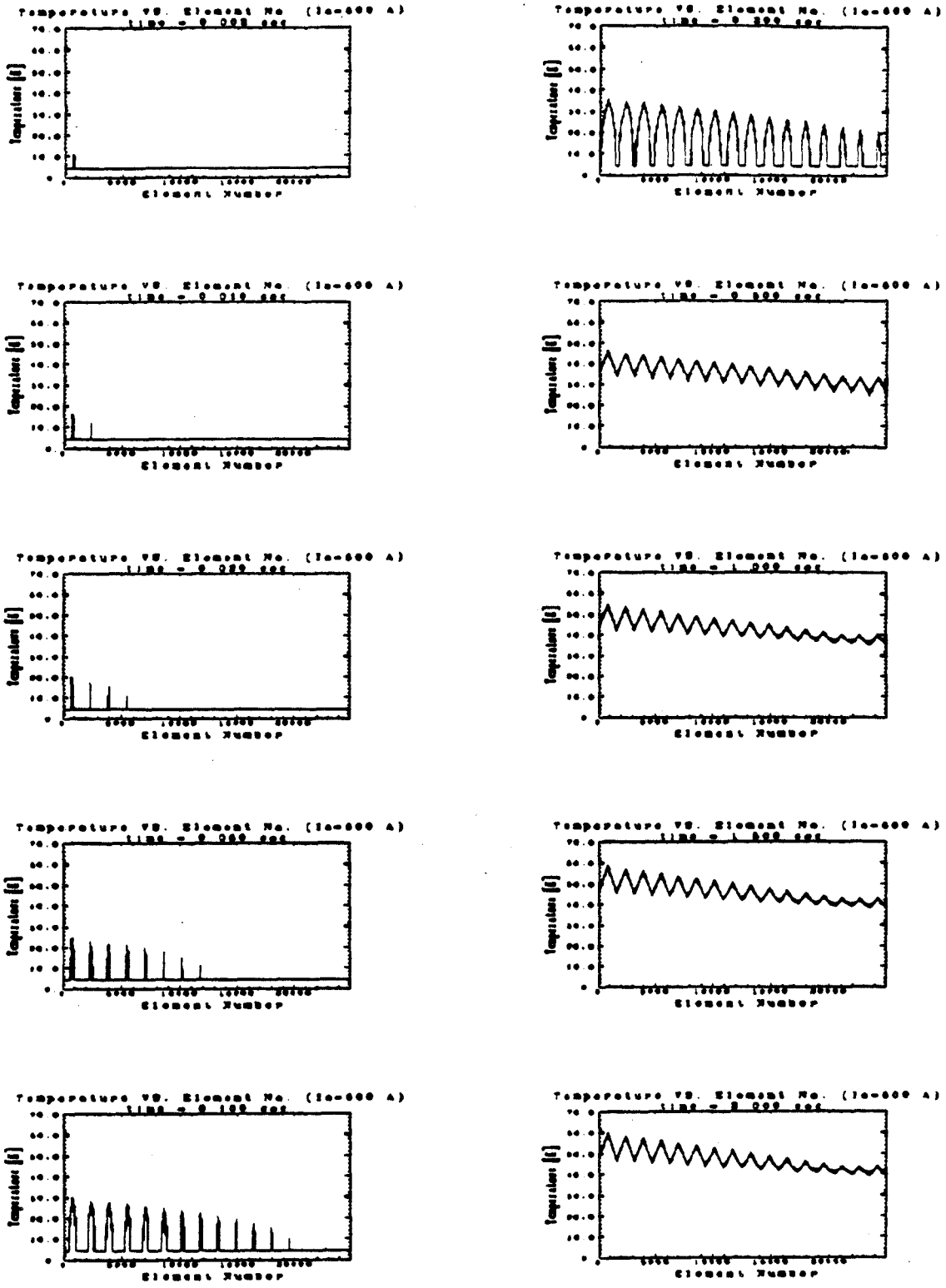

Figure 2.14: Transition of temperature distribution in the coil with respect to element number (1-24960) at an initial current of 600 A for 3–dimensional propagation

transverse propagation conducts faster than the longitudinal propagation to the adjacent elements. At time = 0.2 s (top right picture in Fig. 2.14, all layers have become normal but there are still zones in each layer which are superconducting.

The small ripples in Fig. 2.13 correspond to the transverse quench propagation from turn to turn. More detailed pictures for theses temperature distributions are shown in Fig. 2.15. for the inside layer (element number 1–1560). As shown, the temperature rise from 1.0 s to 2.0 s is slower than that from 0.5 s to 1.0 s because the energy dissipation was lower due to the lower currents toward the end of discharge.

Figures 2.13 and 2.15 show the effect of the magnetic field dependence on the results. Each layer is divided into thirteen regions with magnetic field constant in each region at any given time. The effect of the discrete magnetic field model is to cause a small discontinuity in temperature at the edge of each region. However, the global impact on the results is small.

Figure 2.16 shows the voltage distribution in the coil versus time in a three–dimensional plot. Since the total resistance is rising, the resistive voltage increases for 0.0 to 0.6 s. After the resistive voltage reaches to the maximum value of 38.5 V at time = 0.6 s, it starts to decrease because the current has decayed. Small ripples again correspond to the transverse propagation from turn to turn but are smoother than in the other plots for temperature because the resistive voltage V_R is the integral over all the elements given by:

$$V_R = \sum_{o}^{l_n(t)} I \frac{\rho(B,T) l_n}{A_{mat}} \tag{2.14}$$

where, I is the current, ρ is the resistivity, A_{mat} is the cross-sectional area of the matrix material, and l_n is the length of the normal region at time t.

2.3.2 Analysis of Four-Coil System

Figure 2.17 summarizes the geometry of the four coil system which was analyzed and essential geometry information. The system is composed of one superconducting coil and three normal conducting coils. The normal conducting coils could represent the coil mandrel upon which it is wound.

The construction is the same as described in the previous section, which is an epoxy bonded NbTi superconductor with copper matrix. Thus, the

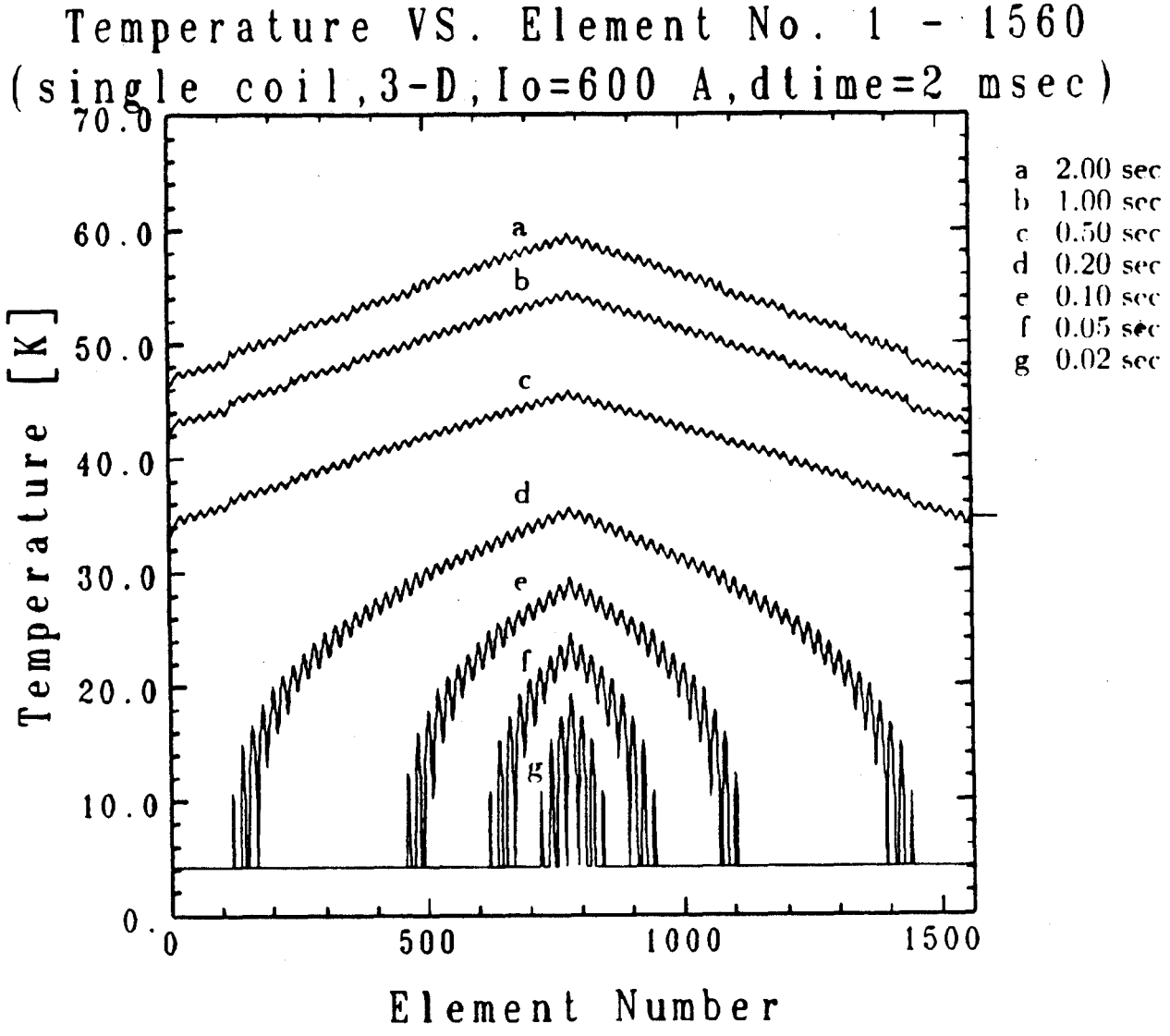

Figure 2.15: Temperature distribution in the inside layer versus element number (1-1560) at an initial current of 600 A for 3-dimensional propagation

Resistive Voltage at an Initial Current of 600 A

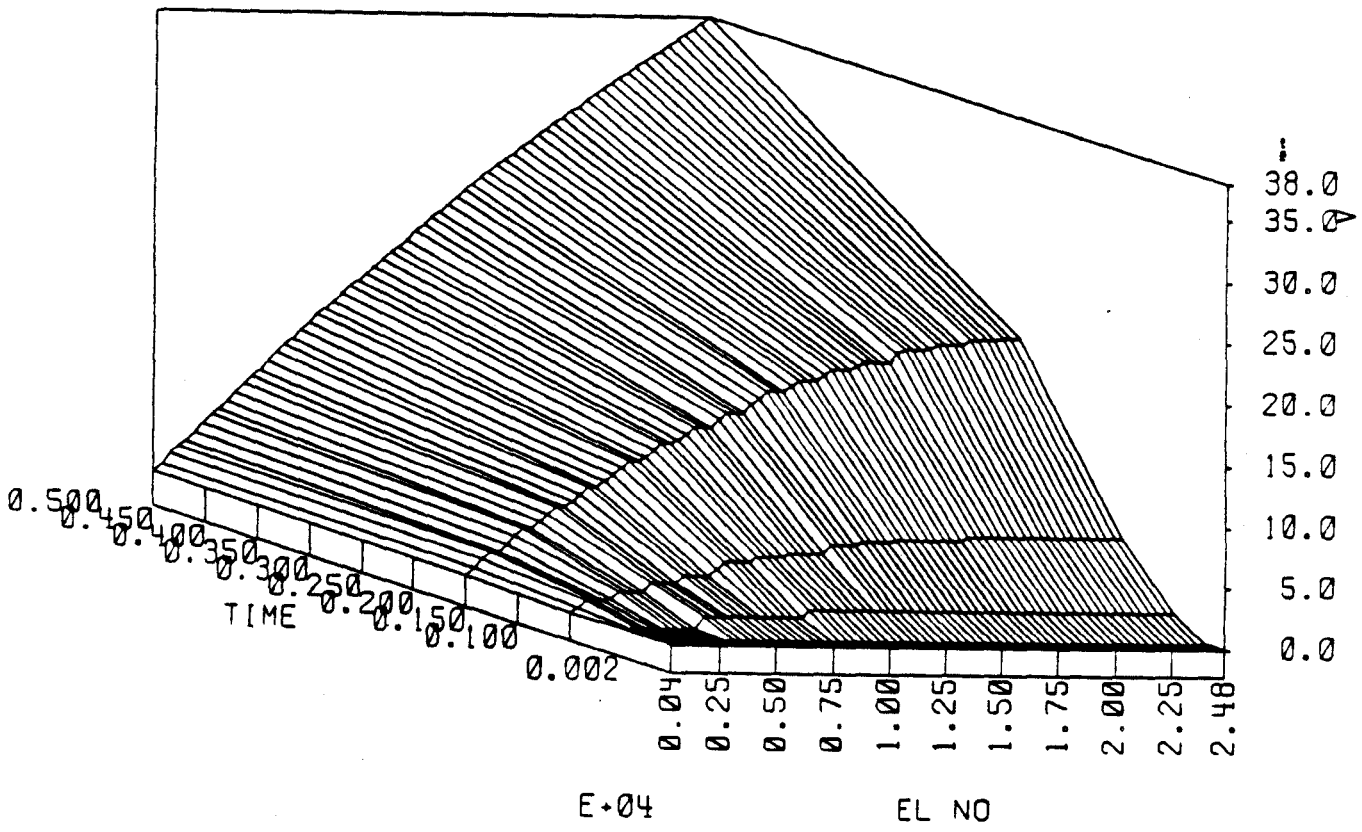

Figure 2.16: Resistive voltage distribution versus element number (1-24960) at an initial current of 600 A for a 3-dimensional propagation

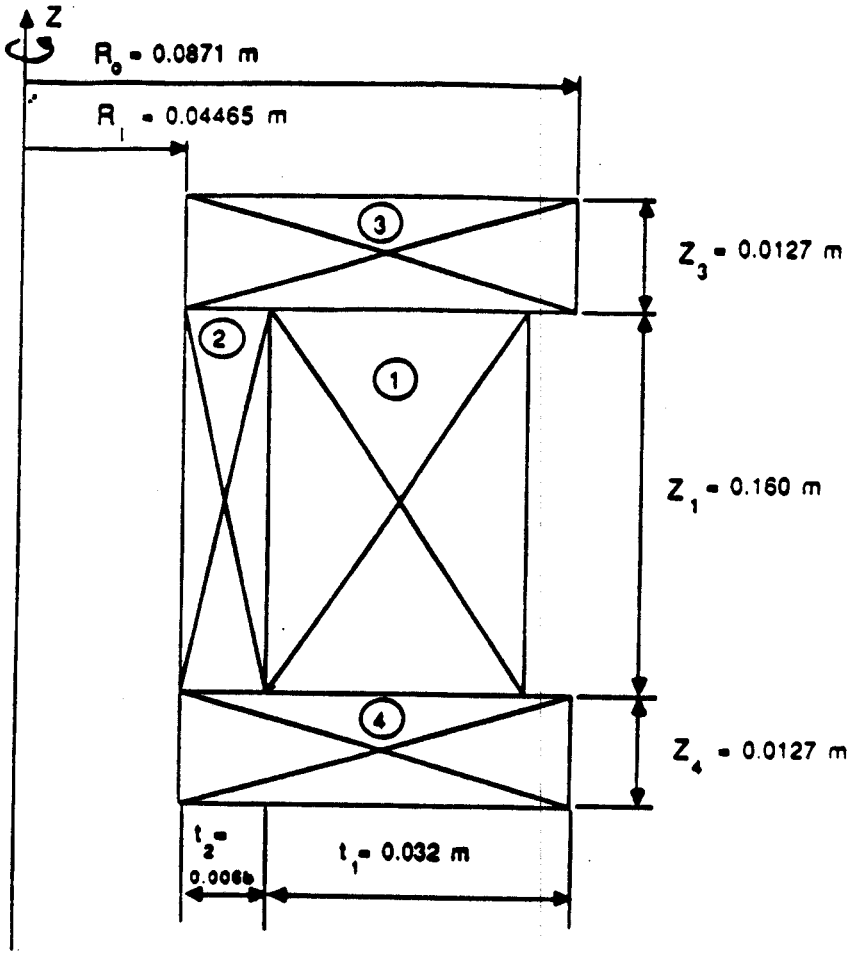

	Coil 1	Coil 2	Coil 3	Coil 4
Magnet Type	superconducting coil epoxy bonded NbTi with Cu matrix	normal conducting coil type 1: 316 S.S. (1) type 2: Cu (2) type 3: Cu/1000 (3)		

(1) resistivity for type 1 (316 S.S.): $\rho = 5.2 \times 10^{-6}\ \Omega$ m

(2) resistivity for type 2 (Cu): $\rho = 1.6 \times 10^{-10}\ \Omega$ m

(3) resistivity for type 3 (Cu/1000): $\rho = 1.6 \times 10^{-13}\ \Omega$ m

Figure 2.17: Geometry of four coil system

characteristics of geometry and material properties for the superconducting coil are also the same. For the normal coils, three cases based on different materials are used: 1) 316 stainless steel (316 S.S.), 2) copper (Cu) and 3) quasi–superconductor whose magnitude of resistivity is 10^{-3} times copper resistivity (designated as Cu/1000 in this section). The purpose of using the type 3 material is to simulate quench propagation behavior in a four coil superconducting system.

The initial current in coil 1 was 600 A. The currents in coils 2, 3 and 4 were zero at the initial time.

As the resistivity of the normal coils becomes smaller in successive cases, the current decay in the coil 1 becomes rapid as shown in Fig. 2.18. This is because the resistivity of coils 2, 3 and 4 affects the current profile in coil 1. More current is induced in the normal coils 2, 3 , and 4 for Cu/1000 than for Cu or for 316 S.S. In particular, for the Cu/1000 case, since all four coils were virtually superconducting material, there was no current decay in coils 2, 3 and 4 because they were not allowed to quench. On the other hand, for the Cu case, the currents in coils 2, 3 and 4 decreased noticeably because of the finite resistance. For the 316 S.S. case, the decrease was fastest.

Figure 2.19 shows the maximum temperature versus time in coil 1. Because of the fast current decay, the temperature in the case for Cu/1000 or for Cu does not become as high as in the single coil situation which is essentially the same as the 316 S.S. case. This multiple coil run showed the tendency to transfer energy from the main coil to other inductively coupled coils and the trend toward lower temperature rise in the quenching coil as the resistivity of the coupled normal coils was reduced.

2.4 Conclusion

A computer program has been developed to simulate quench propagation in multiple superconducting coils by including the following features:

- normal front propagation in the longitudinal and the transverse winding directions;
- magnetic field dependence of material properties for the superconductor and matrix;

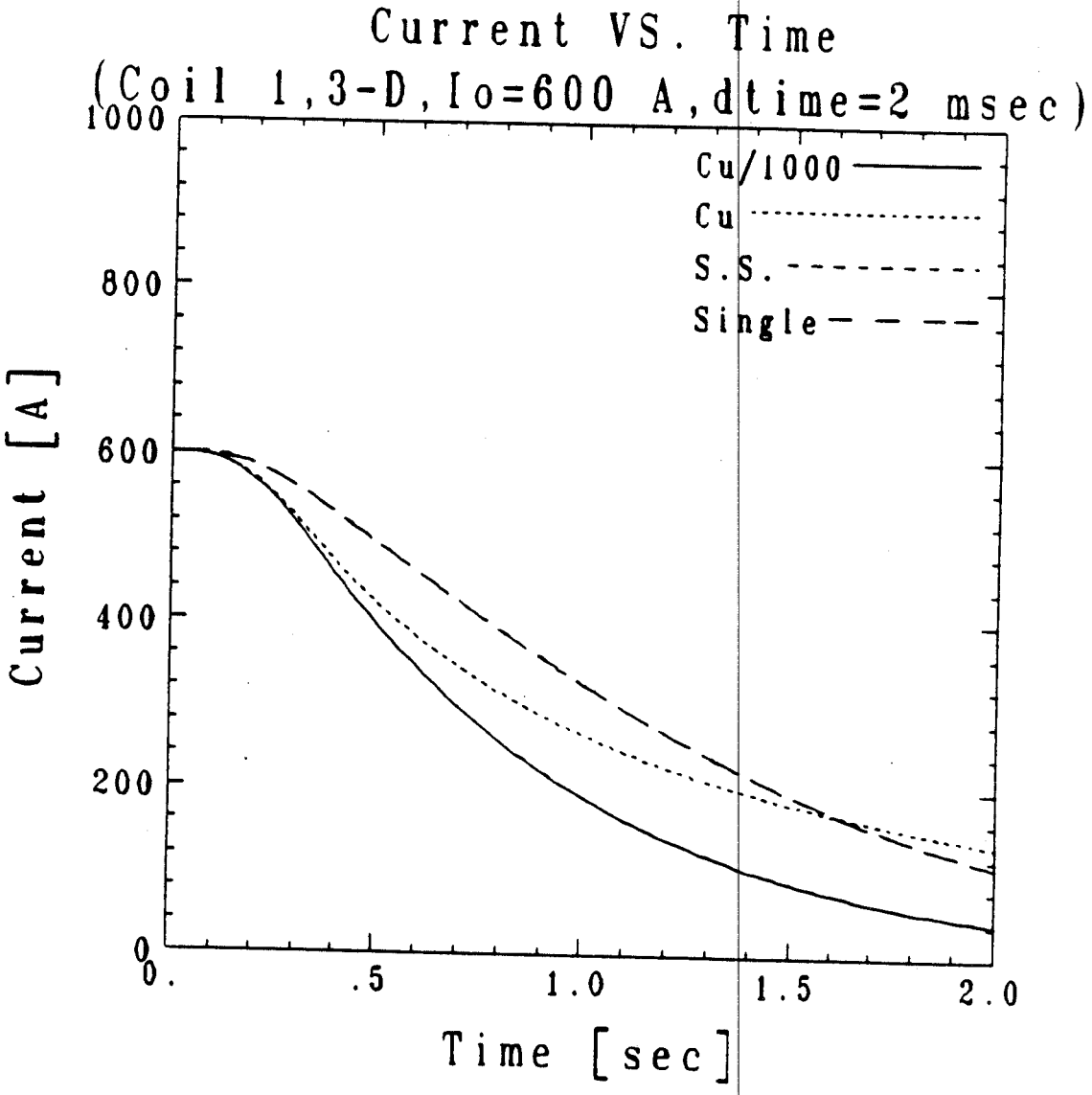

Figure 2.18: Current decay transients in coil 1 for four-coil system with 316 S.S., Cu, and Cu/1000 coils 2, 3 and 4 (Note: The current in coil 1 for the single-coil case is nearly the same as when the other coils are 316 S.S. due to the high resistivity of 316 S.S.)

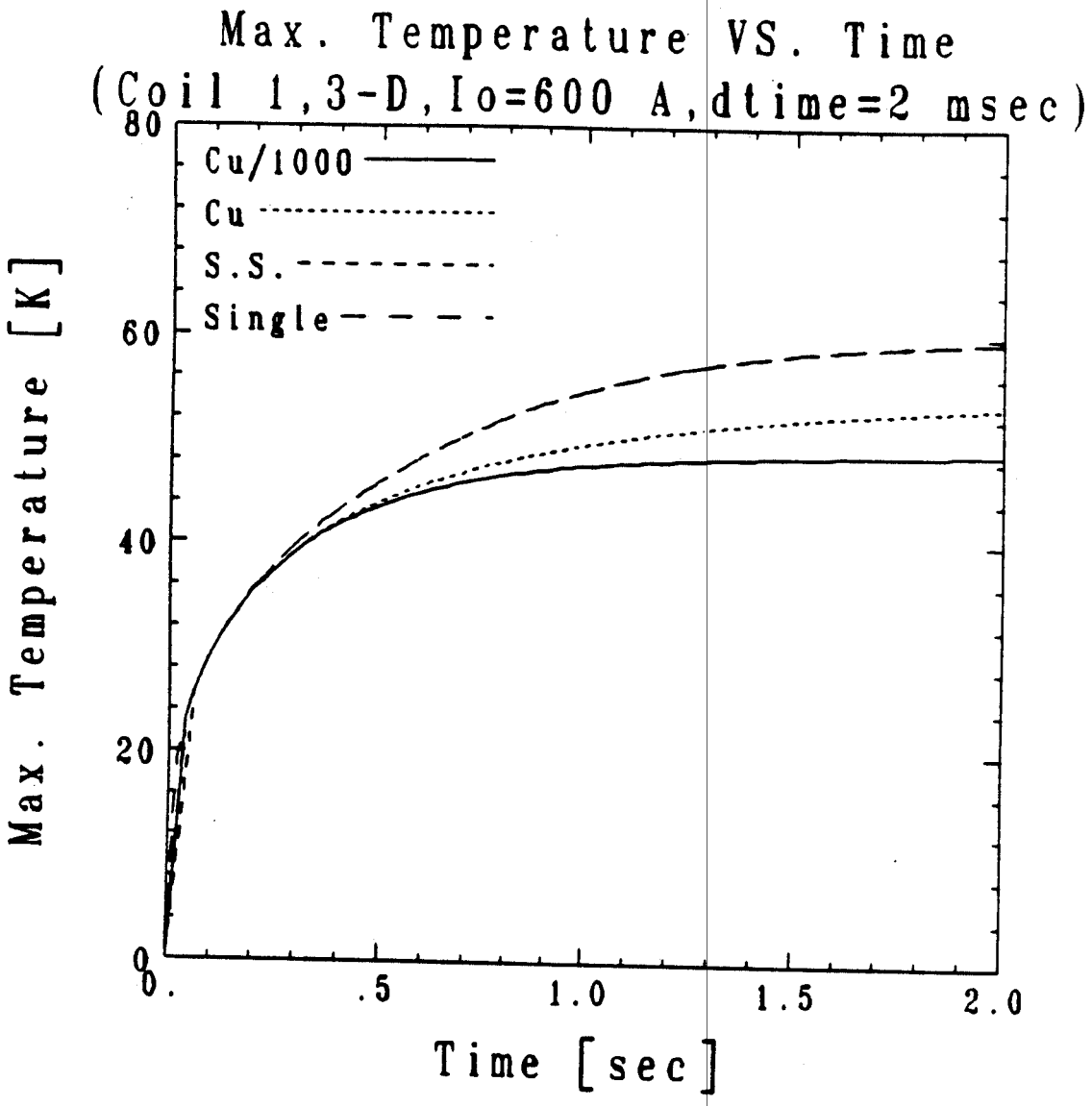

Figure 2.19: Calculated maximum temperature versus time for single coil, 316 S.S., Cu, and Cu/1000 coil 1 (Note: The currents in 316 S.S. coil 1 and single are nearly the same magnitude)

- a logical coordinate system applicable to a general configuration of multiple–coil geometries and multiple–circuits.

The computer program considers the normal region propagation in the longitudinal direction (along the wire conductor) and also in the transverse direction (from turn to turn and from layer to layer through the windings). In order to simulate three-dimensional quench propagation in real space, a logical coordinate system was introduced. In the logical coordinate system, magnets are assumed to be a set of long wires and each wire is divided into finite length elements. Since an element can be associated with geometry–related information such as element length, magnetic field influence coefficients, and relationship to its adjacent elements, quench propagation in any type of configuration can be simplified to a one–dimensional problem.

As the growth of the normal region is determined, the transient current decay can be calculated based on increases in conductor temperature and resistance. This calculation can be done for multiple,inductively coupled systems.

In this thesis, sample analyses of quench propagation were carried out by the computer program "PQUENCH" for two types of coil systems: 1) a single coil system (one NbTi superconductor coil), and 2) a four- coil system (one NbTi superconducting coil and three normal conducting coils).

In the single coil system, computed results showed the importance of the three–dimensional quench propagation on current, voltage and temperature profiles. The computed results were compared with experimental results by using the characteristic quench time τ_o. As a consequence, the computed results show good correlation with the experimental data at high initial currents. However, they begin to deviate at lower initial currents. This is caused by the limited experimental data on the characteristic relation between the critical current and the critical magnetic field, and lack of consideration for the heat conduction between the normal elements.

In order to demonstrate the capability of the program, a four- coil system was simulated. The system consists of one superconducting coil and three normal coils with three different types of resistivity: 1) 316 stainless steel (316 s.s), 2) copper (Cu), and 3) quasi–superconductor whose magnitude of resistivity is 10^{-3} times the resistivity of Cu (designated as Cu/1000). The purpose of using the type 3 normal conductor is to analyze similar behavior in a system of four superconducting coils. The results showed that lowering the

resistivity of the normal coils leads to a higher induced current in the normal coils, and reduces the current in the superconducting coil more rapidly. Thus, to use lower resistivity inductively coupled coils would help protect coil 1 by reducing the temperature rise.

III. Torsional Shear Stress Development in Central Solenoids

3.1 Introduction

One of the fundamental differences between tokamak designs concerns the boundary condition between the outer diameter of the central solenoid and the toroidal field coils.

In a fully "wedged" design, the inboard legs of the TF coils wedge together to produce azimuthal compression as a reaction to the in-plane centering forces on the TF coils. None of the radial centering force on the TF coils is transmitted to the central solenoid, hence the central solenoid is "free standing," that is, the radial stress at its OD is zero. It must contain sufficient structure to equilibrate the radially outward electromagnetic loads that it produces. This is usually done via hoop tension in the windings or structure which may be integral with the windings or external to them. The TF coils and the central solenoid are, essentially, mechanically decoupled.

In a "bucked" design, the inboard legs of the TF coils either do not wedge or partially wedge, and all (or part) of the centering force on the TF coils is transmitted to the OD of the central solenoid. The radially inward load on the central solenoid results in an azimuthal compression which tends to cancel some of the azimuthal tension being produced by the central solenoid self loads. The TF coils and the central solenoid are, as a result, mechanically coupled at the central solenoid OD.

The coupling between the central solenoid and the TF coils in the "bucked" type of design is advantageous for support of the in-plane (i.e., the rz plane) em loads. It leads, however, to other complex interactions which can be the cause of failure. For example, the out-of-plane loads on the TF coils from the poloidal field coils give rise to the so-called overturning moments on the TF coils. The result is a twisting of the TF coils which is partially transmitted to the central solenoid through contact at the interface in a bucked

design. Under some conditions this can lead to high torsional stresses which can shear internal components within the central solenoid.

In this section, we outline the basic concepts underlying the production of the torsional shear stresses within the central solenoid in a bucked design. It can be shown that very little friction at the interface between the TF and the central solenoid is required to effectively lock the surface and lead to torsional shear stresses much higher than the shear stresses at the surface itself. Next year we intend to pursue this model in somewhat more detail in an attempt to relate it to observed effects in actual machines (e.g., JET).

3.2 Torsional Shear Stress

Figure III-1 shows the top half of a central solenoid with a friction coefficient, μ, at its OD. The azimuthal twist of the TF coils (not shown) which are in contact with the central solenoid at the OD, give rise to a shear stress at the interface, $\tau_{r\theta}$. For a central solenoid of half height, h, and radius, R, the torsional shear stress at the midplane and the outer radius of the cylinder may be shown to be $\tau_{z\theta}$ (Eq. III-1). The latter will be a large multiple of $\tau_{r\theta}$ for typical values of h and R.

If the static friction coefficient at the surface is μ, then $\tau_{r\theta}$ and the vertical shear stress, τ_{rz}, are limited to μ times the radial stress at the interface (Eq. III-2). Equation III-3 for the maximum torsional shear stress at the midplane is then obtained by substitution of Eq. III-2 into III-1.

If there is an upper limit to the allowable shear stress in the system, a comparison of Eq. III-2 with III-3 shows that the selection of the allowable friction coefficient at the interface is governed by the $\tau_{z\theta}$ stress. The allowable μ must be considerably lower to provide an upper limit to $\tau_{z\theta}$ because of the geometric multiplier in the system which has the conceptual impact of raising the friction coefficient to a higher effective value.

The model is simple, but illustrates the potential pitfall in which the selection of a friction coefficient to limit shear stresses at the interface ($\tau_{r\theta}$ and τ_{rz}) to a given value, may not be sufficiently low for the torsional shear limit at the midplane of the system. We intend to improve this simple model in the next year to take into account the variation of twist along the interface in the z-direction and the potential benefit of using a compliant layer at the interface which can still transmit the required radial loads but reduce the

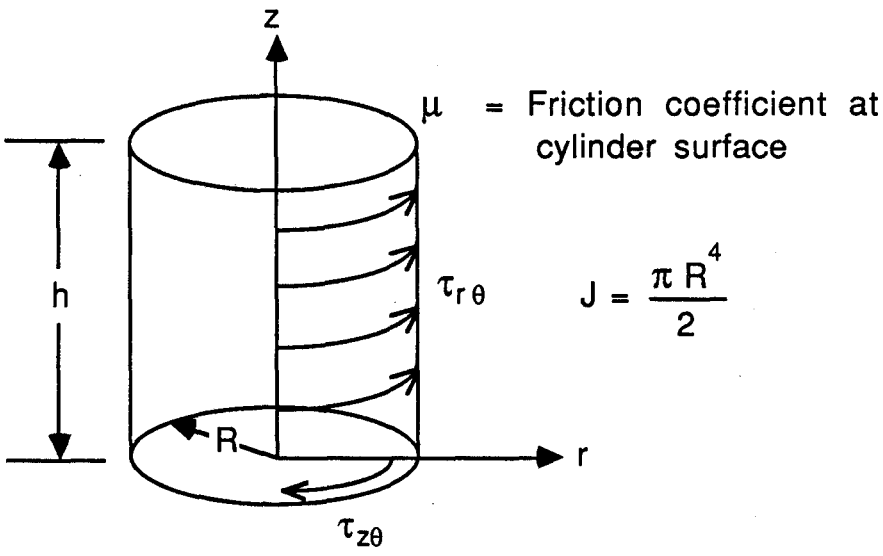

Torque = $\tau_{r\theta}(2\pi R)\,hR = \tau_{z\theta}\frac{J}{R}$

Maximum at r = R

Average over surface

This implies:

$$\tau_{z\theta} = 4\left(\frac{h}{R}\right)\tau_{r\theta} \qquad \text{(III-1)}$$

Shear stress limits on the cylindrical surface are:

$$\tau_{rz} = \tau_{r\theta} = \mu\sigma_{rr} \qquad \text{(III-2)}$$

Limit on torsional shear stress is:

$$\tau_{z\theta} = \underbrace{4\left(\frac{h}{R}\right)}\mu\sigma_{rr} \qquad \text{(III-3)}$$

$\mu_{eff} >> \mu$

Figure III-1 Effective Amplification of Friction Coefficient for Torsional Shear Stress

shear stresses at the coil surface by having a sufficiently low shear modulus.

Bibliography

[1] Oshima, M., "Computation of Quench Propagation in Multiple Superconducting Coils," Engineer's thesis, Nuclear Engineering Department, M.I.T.(1990).

[2] Wilson, M., Superconducting Magnets, Clarendon Oxford Press(1983).

[3] Joshi, C. H., " Thermal and Electrical Characteristics of Adiabatic Superconducting Solenoids During a Spontaneous Transition to the Resistive State," Ph.D thesis, Mechanical Engineering Department, Massachusetts Institute of Technology(1987).

[4] Thome, R. J., Lecture Note for 22.63J, M.I.T., Spring(1989).

[5] Thome, R.J., Magnet Power Supplies and Protection, Lecture Notes for Summer Course on Superconducting Magnet Design, M.I.T, June(1981).

[6] Stekly, Z. J. J., and Thome R. J., "Lightweight Superconducting MHD Magnets - Volume I Saddle Magnet Design, Construction and Preliminary Results," Technical Report AFAPL-TR-72-32, Volume I, June(1972).